

See discussions, stats, and author profiles for this publication at: <https://www.researchgate.net/publication/227180464>

Silver–Gold Nanocomposite Substrates for Metal-Enhanced Fluorescence: Ensemble and Single-Molecule Spectroscopic Studies

ARTICLE in THE JOURNAL OF PHYSICAL CHEMISTRY C · MARCH 2012

Impact Factor: 4.77 · DOI: 10.1021/jp212242x · Source: PubMed

CITATIONS

21

READS

45

4 AUTHORS, INCLUDING:



Sharmistha Dutta Choudhury

47 PUBLICATIONS 668 CITATIONS

[SEE PROFILE](#)



Ramachandram Badugu

80 PUBLICATIONS 2,434 CITATIONS

[SEE PROFILE](#)



Joseph R Lakowicz

University of Maryland Medical Center

875 PUBLICATIONS 41,661 CITATIONS

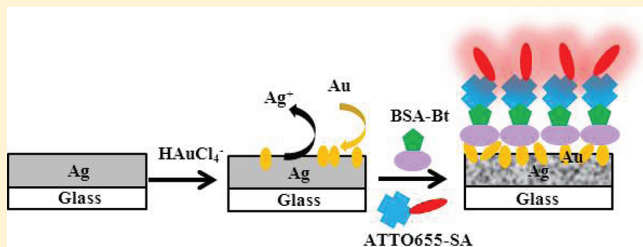
[SEE PROFILE](#)

Silver–Gold Nanocomposite Substrates for Metal-Enhanced Fluorescence: Ensemble and Single-Molecule Spectroscopic Studies

Sharmistha Dutta Choudhury, Ramachandram Badugu, Krishanu Ray, and Joseph R. Lakowicz*

Center for Fluorescence Spectroscopy, Department of Biochemistry and Molecular Biology, University of Maryland Baltimore, 725 West Lombard Street, Baltimore, Maryland 21201, United States

ABSTRACT: In recent years, there has been a growing interest in the studies involving the interactions of fluorophores with plasmonic nanostructures or nanoparticles. These interactions lead to several favorable effects such as increase in the fluorescence intensities, increased photostabilities, and reduced excited-state lifetimes that can be exploited to improve the capabilities of present fluorescence methodologies. In this regard, we report the use of newly developed silver–gold nanocomposite (Ag–Au–NC) structures as substrates for metal-enhanced fluorescence (MEF). The Ag–Au–NC substrates have been prepared by a one-step galvanic replacement reaction from thin silver films coated on glass slides. This approach is simple and suitable for the fabrication of MEF substrates with large area. We have observed about 15-fold enhancement in the fluorescence intensity of ATTO655 from ensemble fluorescence measurements using these substrates. The fluorescence enhancement on the Ag–Au–NC substrates is also accompanied by a reduction in the fluorescence lifetime of ATTO655, which is consistent with the fluorophore–plasmon coupling mechanism. Single-molecule fluorescence measurements have been performed to gain more insight into the metal–fluorophore interactions and to unravel the heterogeneity in the interaction of individual fluorophores with the fabricated substrates. The single-molecule studies are in good agreement with the ensemble measurements and show maximum enhancements of ~50-fold for molecules located in proximity to the “hotspots” on the substrates. In essence, the Ag–Au–NC substrates have a very good potential for various MEF applications.



INTRODUCTION

Fluorescence is one of the dominant detection/sensing methodologies in biological and chemical sciences. For the past several years, we have been working in the exciting area of metal-enhanced fluorescence (MEF), which has the potential to improve the present fluorescence-based techniques such as single-molecule detection, bioimaging, DNA sequencing, or medical diagnostics.^{1–3} MEF is now a well-recognized technology wherein the near-field interaction of fluorophores with metallic colloids or surfaces leads to substantial fluorescence enhancements. This interesting phenomenon results from the combined effects of the creation of an intense excitation field around the metal nanoparticle in the vicinity of the fluorophore, an increase in the intrinsic emission rate of the fluorophore, and a strong coupling between the fluorophore and the plasmons in the metal. The coupled plasmon–fluorophore system can be referred to as the “plasmophore” that radiates into the far-field with increased emission intensity.^{1–3}

Because the fluorophore–plasmon interactions depend on the properties of the metal nanostructures, it is essential to construct robust and reproducible metallic substrates with controlled geometry and tunable optical features, in an easy and cost-effective manner, to realize the full potential of the MEF technique. So far the metallic nanostructures that have been typically used for fluorescence enhancement are based on silver, gold, or aluminum. A number of methods have been developed to fabricate metallic substrates for efficient MEF. These include thermal evaporation,² chemical deposition,² photoinduced depo-

sition,⁴ electrochemical deposition,^{5,6} adsorption of metal colloids on substrates,⁷ lithography,^{8,9} and dealloying.^{10,11} There are also reports of fluorescence enhancements using bimetallic substrates and multilayers composed of solid films and nanoparticles.^{12–15} Xie et al. have demonstrated that Au core–Ag shell nanostructures are promising substrates for fluorescence enhancement with outstanding macroscopic homogeneity.¹⁶ Excellent fluorescence enhancement has been observed by Fu et al. with bimetallic nanopetsals comprised of gold coated silver.¹⁷ Combined gold and silver nanostructured substrates have also been widely investigated for surface-enhanced Raman scattering (SERS), a phenomenon closely related to MEF.¹⁸ In this Article, we report ensemble and single-molecule studies of the MEF using silver–gold nanocomposite (Ag–Au–NC) substrates. The Ag–Au–NC substrates have been fabricated using a simple strategy based on a one-step galvanic replacement reaction of thin silver films coated on glass slides, with gold. The galvanic reaction is reported to be very effective and reproducible for preparing various metallic nanostructures with applications in catalysis and as SERS substrates.^{19–24}

The motivation for this work was two-fold. First, to manipulate the plasmonic properties of the substrate by bringing together the optical properties of gold and silver and second to improve the stability and biocompatibility of silver,

Received: December 19, 2011

Revised: February 2, 2012

Published: February 2, 2012

one of the most widely used metallic substrate for MEF, by combining it with gold nanoparticles. We anticipate that this approach will make the surfaces more suitable for biophysical studies or bio-sensor applications. Furthermore, the preparation of substrates by the simple galvanic replacement reaction removes the need for expensive nanofabrication methods and can be conveniently applied for large-scale substrate production in a cost-effective manner.

With the present Ag–Au–NC substrates, we have observed a significant enhancement in the fluorescence of ATTO655, a dye that is commonly used for bioimaging and single molecule fluorescence based studies. We observed that the increase in the fluorescence intensity of the dye is accompanied by a considerable reduction in its fluorescence lifetime, indicating that the fluorophore-plasmon coupling mechanism is at play. Our ensemble results are well-corroborated by single-molecule fluorescence studies. The single-molecule technique is a very valuable tool to study the intricacies of metal–fluorophore interactions without the averaging effect of ensemble measurements. In the Ag–Au–NC substrate, it is expected that the fluorophore will reside in a variety of locations such as on the tip of a nanoparticle, in the valley between two particles or on the flat surface of a particle. Because the fluorophore–metal interactions depend on the position and orientation of the fluorophore on the metallic surface,^{1–3} there is bound to be heterogeneity in the mode of interaction of individual fluorophores with the metal nanostructures. This can be easily determined from single-molecule studies. Moreover, the fluorophore–metal interaction has the potential to dramatically increase the detectability of single fluorophores by overcoming several limitations of single-molecule spectroscopy such as photostability, low signal intensities, and on–off blinking.^{25–28} Apart from an increase in the fluorophore brightness, the reduced excited-state lifetimes can increase the number of excitation cycles that a molecule can survive before photobleaching. This leads to a significant increase in the number of photons observed from each single molecule.^{25–28} Our experiments confirm that the fabricated Ag–Au–NC substrates enhance the fluorescence of ATTO655 on a molecule-by-molecule basis.

EXPERIMENTAL METHODS

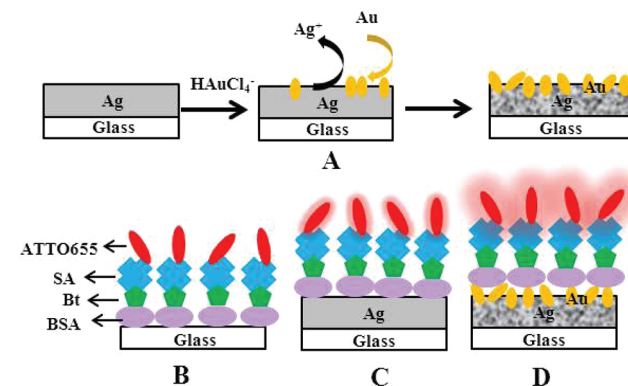
Materials. Silver wire (99.999%), gold(III) chloride trihydrate ($\text{HAuCl}_4 \cdot 3\text{H}_2\text{O}$), biotinylated bovine serum albumin (BSA-Bt), and phosphate buffer (pH 7.4) were purchased from Sigma-Aldrich. The streptavidin conjugated dye; ATTO655-SA, was procured from Invitrogen. Ultrapure water (with a resistivity of $18.2\text{ M}\Omega\text{-cm}$) purified using a Millipore Milli-Q gradient system was used in the preparation of aqueous solutions. Glass microscope slides were obtained from VWR.

Silver–Gold Nanocomposite Substrate Preparation. Glass slides were cleaned with “piranha solution” (35% $\text{H}_2\text{O}_2/\text{H}_2\text{SO}_4$, 1:3) overnight, washed thoroughly with distilled deionized water, and dried with air stream. (Caution: Piranha solution reacts strongly with organic compounds and should be handled with extreme caution. Do not store the solution in a closed container.) Metallic layers were deposited on the cleaned slides using an Edwards Auto 306 Vacuum evaporation chamber under high vacuum ($<5 \times 10^{-7}$ Torr). First, an adhesion layer of chromium was deposited on the slides, which was followed by the deposition of gold (~5 nm) and silver (~600 nm) films, without breaking vacuum. The deposition rate (~1.0 nm/min) was adjusted by the filament current, and the thickness of the metal film was measured with a quartz crystal microbalance. Each metal deposited slide was cut into four equivalent smaller pieces (for convenience in the ensemble and single-molecule fluorescence studies) and immersed in 10 mL of

6 mM HAuCl_4 solution. Spontaneous galvanic replacement of the metallic silver took place with the gold ions in the solution, which was clearly observed from the change in the color of the metal film from shiny silver to brown-gray. The resulting Ag–Au–NC substrates after 15 min of reaction time were then washed with water, dried, and used for further experiments. Scanning electron microscope (SEM) images of these substrates were recorded with a Hitachi SU-70 SEM instrument. An Oxford energy-dispersive X-ray spectrometer (EDS) with silicon drift detector (SSD) attached on the SEM was used for microchemical analysis. Surface morphologies were studied using an atomic force microscope (AFM), Witec Instruments, model alpha300.

Surface Immobilization of ATTO655-SA. The fabricated Ag–Au–NC substrates and glass slides or glass coverslips (used as control) were covered with 100 μL of 1 mg/mL BSA-Bt solution in phosphate buffer and placed in a humid chamber for overnight at 4 °C. Following this step, the slides were washed thrice with phosphate buffer and placed again in a humid chamber. About 60 μL of ATTO655-SA solution (2 μM in buffer) was then placed on the BSA-Bt coated surfaces and incubated for 2 h at room temperature. Finally, the samples were washed multiple times with buffer. The resulting ATTO655-SA monolayer on glass or the Ag–Au–NC surfaces was used for fluorescence measurements. For single-molecule studies, the concentration of ATTO655-SA solution was ~2 nM. A Schematic representation of the Ag–Au–NC substrate fabrication and the immobilization of ATTO655 through the BSA-Biotin-streptavidin chemistry on the different substrates is shown in Scheme 1. The surfaces were always kept

Scheme 1. Schematic Representation of Ag–Au–NC Substrate Fabrication (A) and the Immobilization of ATTO655 on (B) Glass, (C) Ag Film, and (D) Ag–Au–NC Substrates through the BSA-Biotin-Streptavidin Chemistry



under the wet condition while performing the experiments to avoid protein unfolding or denaturation by drying. All comparative studies between the fabricated Ag–Au–NC substrates and the glass slides were made under identical experimental conditions. The biotin–streptavidin assembly, used in the present case, not only helps in the immobilization of a monolayer of fluorophore on the surfaces but also places the fluorophore at a suitable distance (~9 nm) from the metallic surface for efficient MEF.²⁹

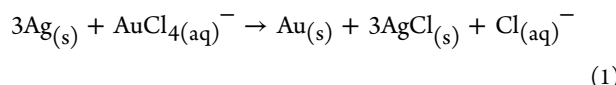
Ensemble Fluorescence Measurements. Ensemble emission spectra of ATTO655-SA on the solid substrates were obtained using a Varian Cary Eclipse fluorescence spectrophotometer. Both the steady-state and time-domain lifetime measurements were carried out using front face illumination. Bandpass interference filters were used to minimize the scattered light at the excitation wavelength. The fluorescence lifetimes were recorded

using a time-correlated single photon counting (TCSPC) instrument (PicoQuant, FluoTime 100). The excitation source was a pulsed laser diode (635 nm, 20 MHz repetition rate using PDL800-B), with an instrument response function of ~ 300 ps. The fluorescence decays were collected at magic angle with respect to the vertically polarized excitation light. The FluorFit software from PicoQuant was used for the analysis of the observed fluorescence decays. With the present TCSPC setup, fluorescence lifetimes as short as 60 ps could be recovered from the deconvolution analysis.

Single-Molecule Imaging and Lifetime Studies. The single-molecule studies were performed with a confocal microscope (PicoQuant, MicroTime 200) equipped with TCSPC capabilities (TimeHarp 200 PCI-board). A pulsed laser diode (635 nm, 100 ps, 40 MHz) was used as the excitation source. The excitation laser was directed through a 10 nm bandpass excitation filter and reflected by a dichroic mirror (Z470/635rpc) into an inverted microscope (Olympus, IX 71). An oil immersion objective (Olympus 100 \times , 1.3 NA) was used for focusing the laser light onto the sample and for collecting the fluorescence emission from the sample. The fluorescence signal that passed through the dichroic mirror and a long-pass filter (Q65SLP, Chroma) was focused through a 75 μm pinhole to a single-photon avalanche photodiode (SPAD) detector. Images were recorded by raster scanning (in a bidirectional manner) the sample over the focused spot of the incident laser with a pixel integration of 0.6 ms. The excitation power was maintained at less than 2 μW . Intensity-time trajectories and intensity-time decays were obtained by positioning the excitation beam over individual ATTO655-SA molecules. The data were stored in the time-tagged time-resolved mode that allows recording every detected photon with its individual timing information. Lifetimes were estimated by fitting to a χ^2 value of less than 1.2 and a residual trace that was symmetrical about the zero axis. For acquiring single-molecule emission spectra, the Microtime 200 has been coupled to a spectrograph (Princeton Instruments, Acton) consisting of high reflectance mirrors, 150G/mm dispersion grating with 500 nm blaze wavelength and having efficient imaging from 450 to 750 nm. An electron-multiplied CCD (Princeton Instruments photon Max 512) with high quantum efficiency (>90% visible range) was used as the detector.

RESULTS AND DISCUSSION

The Ag–Au–NC nanocomposites have been conveniently prepared by the galvanic replacement of metallic silver with gold ions. Figure 1A,B shows representative SEM images of the vacuum-deposited silver substrate before and after the reaction with HAuCl₄ for 15 min. A clear transformation from a flat and uniform surface to a substantially rough and structured morphology, having particle sizes ranging from ~ 200 nm to 1 μm , can be observed. This change in morphology results from the highly favorable replacement reaction between Ag and Au³⁺.^{19,20} Because the reduction potential of AuCl₄⁻/Au (0.99 V vs standard hydrogen electrode, SHE) is higher than that of Ag⁺/Ag (0.8 V vs SHE), elemental silver can be oxidized by HAuCl₄ according to the following reaction



This leads to the facile formation and deposition of nanoscale Au particles uniformly distributed on the surface of the sacrificial Ag substrate. The reaction also produces AgCl, which being insoluble in the aqueous solution, crystallizes on the

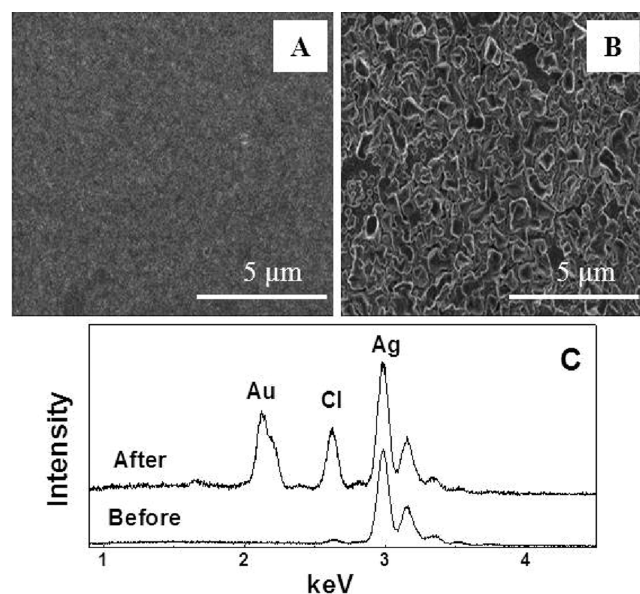


Figure 1. SEM images of the thermally evaporated Ag film before (A) and after (B) reaction with HAuCl₄ for 15 min and their EDS spectra (C).

substrate in the form of microparticles.^{19,20,30} Moreover, depending on the reaction time and the concentration of HAuCl₄, a fraction of the unreacted Ag remains on the metal film, leading to the generation of desired Ag–Au–NC substrates. The EDS analysis performed on the as-fabricated substrates (Figure 1C) yields an elemental composition of Au (26%), Ag (64%), and Cl (10% by weight), which is in accordance with the reaction (eq 1). The AgCl that is codeposited on the substrate as a byproduct of the reaction can be removed by washing the nanocomposite samples with concentrated NaCl solution.^{19,30} However, no significant differences were observed in our subsequent fluorescence studies using the Ag–Au–NC substrates, with or without the treatment with NaCl.

The presence of residual metallic silver on the fabricated substrates is advantageous because silver is known to have suitable plasmonic properties for MEF. However, silver surfaces are prone to oxidation and are relatively unstable. Gold surfaces are resistant to oxidation, are in general more stable, and have favorable surface chemistry. So it is expected that the fabricated substrates with surface-deposited gold nanoparticles will provide a more robust surface, while at the same time the residual silver will provide favorable metal–fluorophore interactions for better fluorescence enhancement. A favorable effect of the residual silver has recently been reported by Zhang et al. in the SERS effect of dealloyed nanoporous gold.³¹ In the present study, the Ag–Au–NC substrates prepared with a reaction time of 15 min are found to show maximum fluorescence enhancements. With further increase in galvanic replacement reaction time, the amount of residual silver present in the substrate gradually decreases, and consequently the MEF effect of the substrate also reduces.

In addition to the SEM imaging that gives information on the lateral dimensions of the Ag–Au–NC substrates, AFM was used for gathering information on the axial dimensions and morphology of the nanostructures (Figure 2). The line profile across the AFM image indicates the height of the nanostructures to be in the range of 200–500 nm.

The probe immobilization procedure used in the present study is shown in Scheme 1 and is described in the Experimental Section. Figure 3A shows the emission spectra of ATTO655-SA

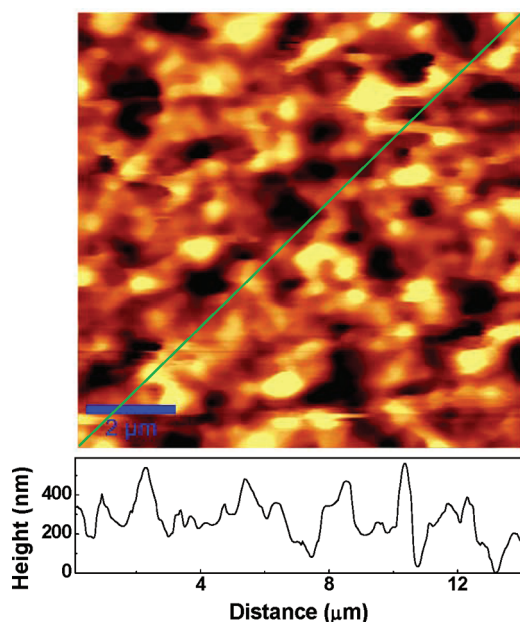


Figure 2. AFM image ($10 \mu\text{m} \times 10 \mu\text{m}$) and a line profile across the Ag–Au–NC substrate.

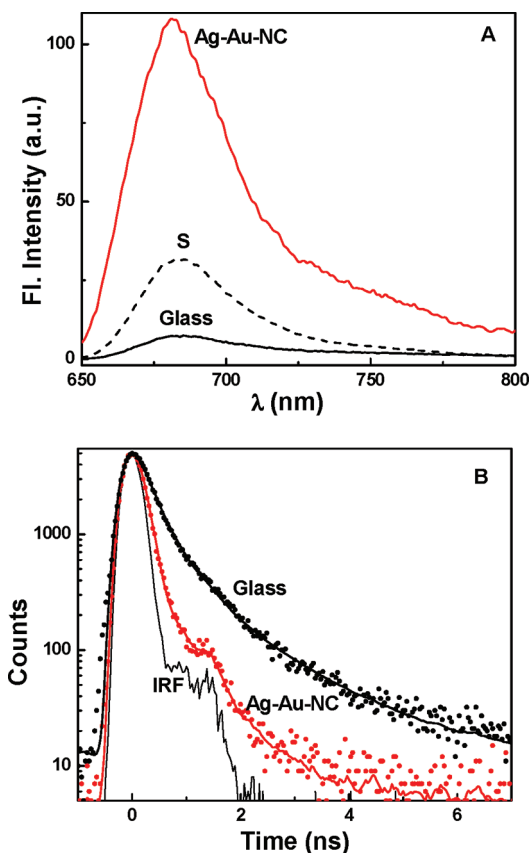


Figure 3. (A) Fluorescence emission spectra of ATTO655-SA on glass, the thermally evaporated Ag film before the galvanic reaction (s) and the Ag–Au–NC substrate. (B) Fluorescence decay traces of ATTO655-SA on glass and Ag–Au–NC substrate.

immobilized on the fabricated Ag–Au–NC substrates and on bare glass slides, used as the control. The emission spectrum on the starting Ag substrate (prior to the galvanic replacement reaction) is also shown for comparison. The nature of the probe emission

spectra on all of the substrates is similar with maximum around 683 nm. About 15-fold enhancement in the fluorescence intensity of ATTO655-SA is observed on the Ag–Au–NC substrate in comparison with that from the probe on bare glass. The corresponding enhancement from the starting Ag substrate is about five-fold. This result immediately suggests the superior performance of the fabricated Ag–Au–NC substrate as compared with the Ag-film itself. In general, planar metallic films (Ag or Au) do not show significant fluorescence enhancements because they cannot support localized surface plasmon polaritons. The localized surface plasmon polaritons on metallic nanostructures are largely responsible for the substantial increase in the excitation fields and hence the increase in the fluorescence intensities of vicinal fluorophores. The deposition of Au nanoparticles by the galvanic reaction thus improves the fluorescence enhancement capability of the Ag–Au–NC substrate (Figure 3A). However, to understand whether this fluorescence enhancement arises due to the fluorophore-plasmon coupling effect or whether it is merely due to the increased excitation fields near metallic substrates, it is necessary to examine the excited-state lifetime of ATTO655-SA on the fabricated substrates.

The fluorescence intensity decay traces for ATTO655-SA on glass and Ag–Au–NC substrate are shown in Figure 3A. The decay traces on both the substrates can be fitted to biexponential functions. The average fluorescence lifetime of the dye on the glass substrate is ~ 0.5 ns. The biexponential nature of the fluorescence decay on the glass substrate may be effected by intramolecular electron transfer from the tryptophan moieties of streptavidin to the excited ATTO655 in the streptavidin-conjugated dye, ATTO655-SA.³² It is also observed that the fluorescence lifetime of ATTO655-SA is much shorter on the glass substrate in comparison with that in aqueous solutions (~ 1.7 ns).³² This can be explained on the basis of the differences in the conformations of ATTO655-SA on the solid substrate and in solution. A change in the conformation of the protein can significantly influence the intramolecular electron transfer between the tryptophan residues and ATTO655 and hence can affect the excited-state lifetime of the dye.³²

On the Ag–Au–NC substrate, the average fluorescence lifetime of ATTO655-SA is further shortened to ~ 0.16 ns. The reduction in the fluorescence lifetime of the fluorophore despite an increase in the fluorescence intensity is a characteristic feature of the fluorophore-plasmon coupling effect.^{1–3} This behavior is quite contrary to the free-space condition where both the fluorescence intensity and lifetime change in unison. Therefore, the opposing effect of the Ag–Au–NC substrate on the fluorescence intensity and the excited-state lifetime of ATTO655-SA clearly suggests a plasmon-induced increase in the radiative decay rate of the fluorophore. It is interesting to note that the enhancement in the steady-state fluorescence intensity (~ 15 -fold) is much larger in comparison with the reduction in the average fluorescence lifetime (approximately three-fold) of ATTO655-SA on the Ag–Au–NC substrates. This indicates that in addition to the near-field fluorophore-plasmon coupling effect, the increased excitation fields in the vicinity of the substrate also contribute to the net fluorescence enhancement to some extent. It can also be argued that the fluorescence enhancement on the nanocomposite substrates arises because of an increased surface area and hence an increased fluorophore concentration on these substrates in comparison with that on the bare glass. This issue can be resolved by performing single-molecule fluorescence studies (discussed below).

Figure 4A,B presents $20 \times 20 \mu\text{m}$ confocal fluorescence images of ATTO655-SA immobilized on a clean glass coverslip and on the Ag–Au–NC substrate, respectively. The well-separated

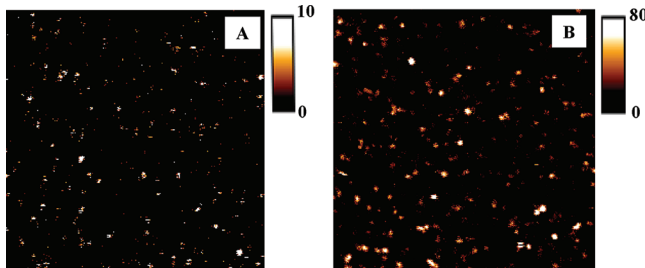


Figure 4. Scanning confocal images ($20 \mu\text{m} \times 20 \mu\text{m}$) of ATTO655-SA on (A) glass and (B) Ag–Au–NC substrate. Scale bars show the respective intensity counts in 0.6 ms bin.

bright spots in the images represent fluorescence emission from single-dye molecules. The increase in the brightness of individual ATTO655-SA molecules on the Ag–Au–NC substrates is clearly evident from these images. This observation undoubtedly proves that the enhanced fluorescence intensity on the fabricated substrates is not a result of the increased probe concentration due to increased surface area of these substrates in comparison with bare glass but is due to the MEF effect.

To have more insight into the underlying photophysics of single ATTO655-SA molecules on glass and on the Ag–Au–NC surfaces, the fluorescence intensity of individual dye molecules were monitored under constant illumination. Representative intensity–time trajectories of four different ATTO655-SA molecules bound to glass or Ag–Au–NC surfaces are presented

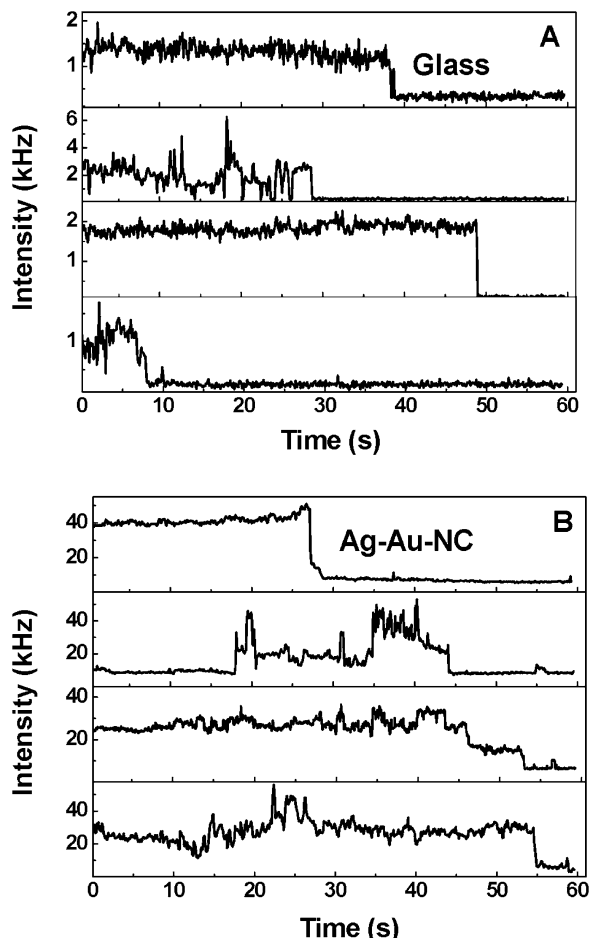


Figure 5. Intensity–time trajectories of individual ATTO655-SA molecules on (A) glass and (B) Ag–Au–NC substrate.

in Figure 5A,B, respectively. The fluorescent spots showed blinking and single-step photobleaching in both the substrates, corresponding to the typical behavior that is expected for a single molecule. Interestingly, much larger fluctuations in the fluorescence intensities are observed for the ATTO655-SA on the Ag–Au–NC substrate in comparison with glass, prior to photobleaching. This fluctuation in the fluorescence intensity can be attributed to the flexibility of the ATTO655 molecules that are tethered to the surface by the biotin-streptavidin chemistry. It is known that the metal–fluorophore coupling depends on the distance and orientation of the fluorophore transition dipole with respect to the metallic substrate. So any conformational fluctuations can markedly influence the plasmonic coupling and hence the ensuing fluorescence enhancement, thus leading to the variation in the fluorescence intensity.^{1–3,33}

It is known that silver and gold nanoparticles can be photoactivated with light and display characteristic blinking behavior.^{34,35} Strong intensity fluctuations and nondestructive blinking have been reported for silver nanoparticles under continuous illumination.³⁵ This could lead to complications in single-molecule spectroscopic studies. However, the blinking behavior from single organic dye molecules is very different from metal nanoparticles and can be distinguished from the latter. To confirm that the fluorescence spots on the Ag–Au–NC substrate arise from single-dye molecules and not from the nanoparticle luminescence, single-molecule emission spectra have been recorded. The emission spectra of single ATTO655-SA

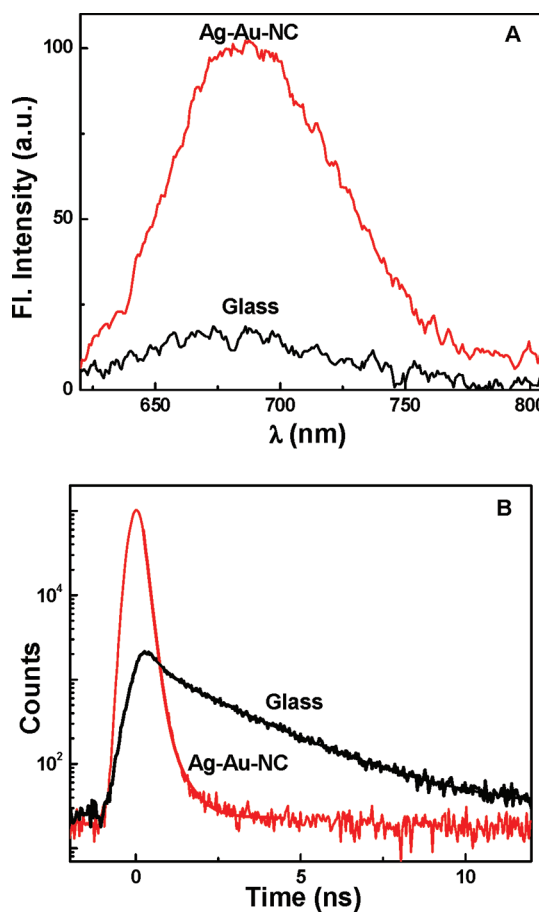


Figure 6. (A) Single-molecule fluorescence spectra of individual ATTO655-SA on glass and Ag–Au–NC substrate. (B) Fluorescence intensity decays of individual ATTO655-SA on glass and Ag–Au–NC substrate.

molecules on the Ag–Au–NC substrate are similar to those observed from ensemble measurements and show fluorescence enhancement in comparison with that on glass. Representative spectra are shown in Figure 6A. Typical single-molecule intensity decays of individual ATTO655-SA molecules on the nanocomposite substrate and glass are shown in Figure 6B. A dramatic reduction in the lifetime is observed on the Ag–Au–NC substrate, which is in good agreement with the MEF phenomenon.

To understand the heterogeneity in the brightness and lifetimes of individual ATTO655-SA molecules on the Ag–Au–NC and glass substrates, intensity and average fluorescence lifetime histograms were constructed for multiple (~70) single dye molecules (Figure 7). Only those spots that show single-step photobleaching have been considered in this analysis to avoid any complications from metal nanoparticle luminescence. Examination of the intensity histograms shows that the ATTO655-SA molecules have an average intensity of about 48 kHz on the Ag–Au–NC substrate and ~4 kHz on glass (Figures 7A,B). Some of the molecules on the nanocomposite substrate are observed to be very bright (~100–140 kHz) that is nearly 50-fold brighter than that from the glass surface. It is possible that these molecules reside in the “hotspots” on the nanocomposite substrate, where the fluorophore–plasmon

coupling is very efficient. Such plasmonic hotspots, often the nanoscale clefts, gaps, or fissures in nanostructured metals, are known to amplify the electromagnetic fields to a very large extent.^{36,37} We also observe that the relative standard deviation of the intensity distribution is higher on the Ag–Au–NC substrate (~62%) than on glass (~52%).

From the lifetime distributions, the average fluorescence lifetime of ATTO655-SA molecules on the Ag–Au–NC substrate is found to be much shorter (~0.3 ns), as expected, than the average lifetime on glass, ~1.9 ns (Figures 7C,D). However, the average fluorescence lifetime on glass is observed to be longer (~1.9 ns) from the single-molecule study in comparison with the ensemble measurements (0.5 ns). This can be attributed to the fact that only the bright ATTO655-SA molecules have been detected on the glass substrate in the single-molecule measurements. The molecules that are quenched by the intramolecular electron transfer from the tryptophan moieties of streptavidin and have shorter lifetimes are not observed in the single-molecule measurements and thus have not been considered for the statistical analysis of the lifetime distribution histograms.

As in the case of the intensity distributions, a relatively high standard deviation of ~50% is observed for the lifetime distributions on the Ag–Au–NC substrate compared with that

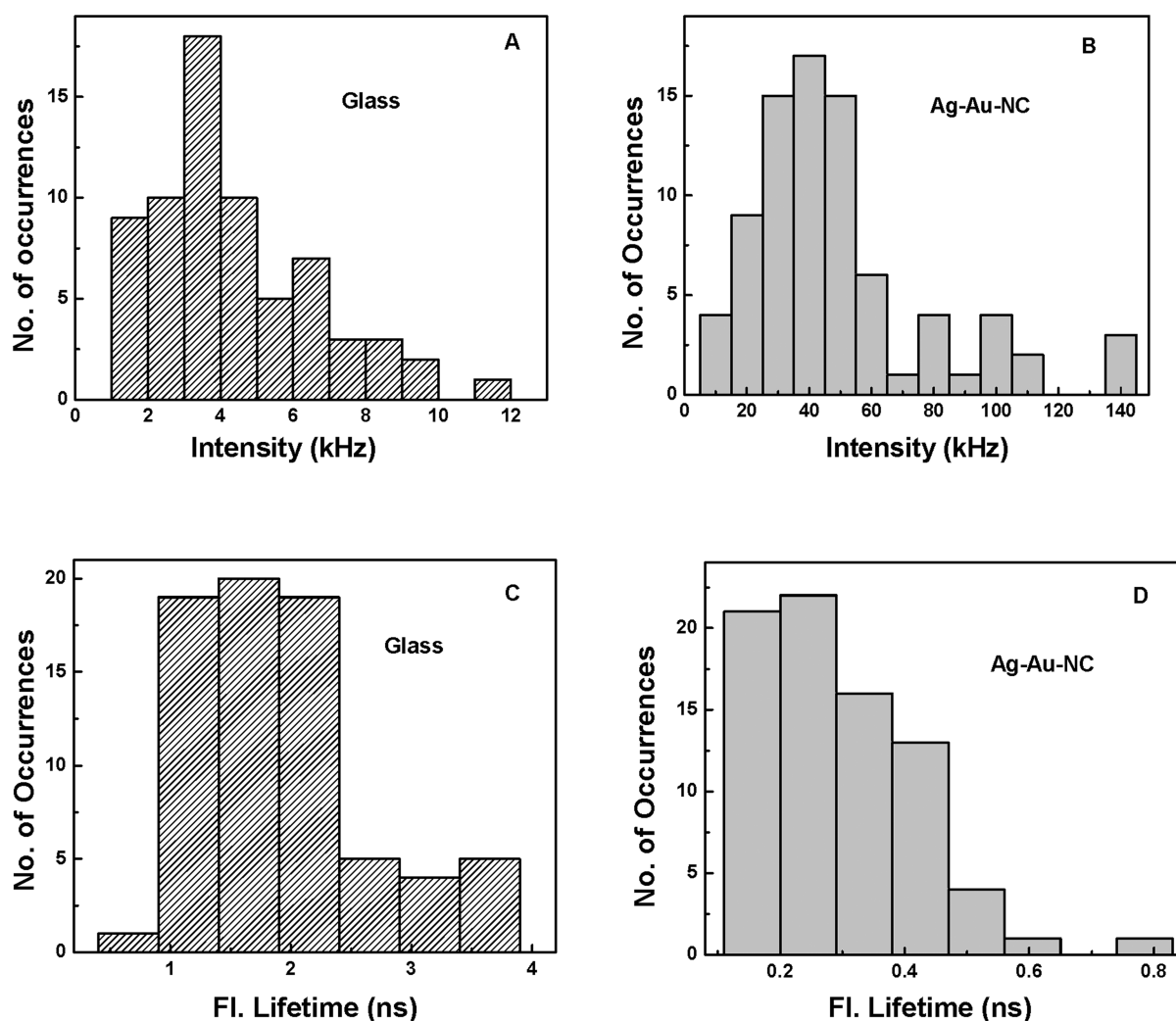


Figure 7. Fluorescence intensity (count rate) histogram of ATTO655-SA on (A) glass and (B) Ag–Au–NC substrate. Average fluorescence lifetime histogram of ATTO655-SA on (C) glass and (D) Ag–Au–NC substrate. The histograms have been constructed for ~70 single molecules in each case.

on glass (~38%). The heterogeneity on the glass substrate mainly arises due to the different conformations of the streptavidin moiety in the immobilized ATTO655-SA molecules. As previously mentioned, the variations in the conformation of streptavidin can affect the intramolecular electron transfer in ATTO655-SA and lead to differences in the fluorescence intensities and lifetimes of individual fluorophores.³² On the Ag–Au–NC substrate, in addition to this effect, there is also a site-to-site variation in the local electromagnetic field and thus overall interactions between the fluorophore and plasmonic metal nanocomposites. This leads to a much wider distribution in the fluorescence intensities and lifetimes on the nanocomposite substrate.

CONCLUSIONS

In summary, this work reports the facile and easy fabrication of large area Ag–Au–NC substrates that are suitable for efficient MEF-based studies. About 15-fold enhancement in the fluorescence intensity of ATTO655-SA at ensemble level has been observed using the present substrates. This is accompanied by an approximately three-fold decrease in the fluorescence lifetimes, which suggests that the near-field fluorophore-plasmon coupling effect is responsible for the fluorescence enhancement. The ensemble studies are in agreement with those from the single-molecule measurements. The single-molecule study provides further insight into the heterogeneity in the fluorescence enhancement and lifetimes of the ATTO655-SA molecules on both glass and the nanocomposite substrates, which cannot be observed using ensemble measurements.

AUTHOR INFORMATION

Corresponding Author

*E-mail: jlakowicz@umaryland.edu.

Notes

The authors declare no competing financial interest.

ACKNOWLEDGMENTS

S.D.C. acknowledges the Indo-US Science and Technology Forum (IUSSTF) for the grant of the IUSSTF Fellowship. We also acknowledge the support of the Maryland NanoCenter and its FabLab. This work was supported by the National Institutes of Health (NIH), Grants R01HG002655, and K25AI087968.

REFERENCES

- (1) Lakowicz, J. R. *Anal. Biochem.* **2001**, *298*, 1.
- (2) Lakowicz, J. R.; Shena, Y.; D'Auria, S.; Malicka, J.; Fang, J.; Gryczynski, Z.; Gryczynski, I. *Anal. Biochem.* **2002**, *301*, 261.
- (3) Lakowicz, J. R.; Ray, K.; Chowdhury, M.; Szmacinski, H.; Fu, Y.; Zhang, J.; Nowaczky, K. *Analyst* **2008**, *133*, 1308.
- (4) Geddes, C. D.; Parfenov, A.; Roll, D.; Fang, J.; Lakowicz, J. R. *Langmuir* **2003**, *19*, 6236.
- (5) Goldys, E. M.; Drozdowicz Tomsia, K.; Xie, F.; Shtyko, T.; Matveeva, E.; Gryczynski, I.; Gryczynski, Z. *J. Am. Chem. Soc.* **2007**, *129*, 12117.
- (6) Parfenov, A.; Gryczynski, I.; Malicka, J.; Geddes, C. D.; Lakowicz, J. R. *J. Phys. Chem. B* **2003**, *107*, 8829.
- (7) Xie, F.; Baker, M. S.; Goldys, E. M. *Chem. Mater.* **2008**, *20*.
- (8) Pompa, P. P.; Martiradonna, L.; Della-Torre, A.; Carbone, L.; delMercato, L. L.; Manna, L.; De Vittorio, M.; Calabi, F.; Cingolani, R.; Rinaldi, R. *Sens. Actuators, B* **2007**, *127*, 187.
- (9) Shiv Shankar, S.; Rizzello, L.; Cingolani, R.; Rinaldi, R.; Pompa, P. P. *ACS Nano* **2009**, *3*, 893.
- (10) Lang, X. Y.; Guan, P. F.; Fujita, T.; Chen, M. W. *Phys. Chem. Chem. Phys.* **2011**, *13*, 3795.
- (11) Ahl, S.; Cameron, P. J.; Liu, J.; Knoll, W.; Erlebacher, J.; Yu, F. *Plasmonics* **2008**, *3*, 13.
- (12) Matveeva, E. G.; Gryczynski, I.; Barnett, A.; Leonenko, Z.; Lakowicz, J. R.; Gryczynski, Z. *Anal. Biochem.* **2007**, *363*, 239.
- (13) Sørensen, T. J.; Laursen, B. W.; Luchowski, R.; Shtyko, T.; Akopova, I.; Gryczynski, Z.; Gryczynski, I. *Chem. Phys. Lett.* **2009**, *476*, 46.
- (14) Szmacinski, H.; Badugu, R.; Lakowicz, J. R. *J. Phys. Chem. C* **2010**, *114*, 21142.
- (15) Chowdhury, M. H.; Chakraborty, S.; Lakowicz, J. R.; Ray, K. *J. Phys. Chem. C* **2011**, *115*, 16879.
- (16) Xie, F.; Baker, M. S.; Goldys, E. M. *J. Phys. Chem. B* **2006**, *110*, 23085.
- (17) Fu, C.; Ossato, G.; Long, M.; Digman, M. A.; Gopinathan, A.; Lee, L. P.; Gratton, E.; Khine, M. *Appl. Phys. Lett.* **2010**, *97*, 20310.
- (18) Oates, T. W. H.; Shiratori, Y.; Noda, S. *J. Phys. Chem. C* **2009**, *113*, 9588.
- (19) Sun, Y.; Xia, Y. *J. Am. Chem. Soc.* **2004**, *126*, 3892.
- (20) Au, L.; Lu, X.; Xia, Y. *Adv. Mater.* **2008**, *20*, 2517.
- (21) Mohl, M.; Kumar, A.; Reddy, A. L. M.; Kukovecz, A.; Konya, Z.; Kiricsi, I.; Vajtai, R.; Ajayan, P. M. *J. Phys. Chem. C* **2010**, *114*, 389.
- (22) Bansal, V.; Jani, H.; Plessis, J. D.; Coloe, P. J.; Bhargava, S. K. *Adv. Mater.* **2008**, *20*, 717.
- (23) Gutés, A.; Carraro, C.; Maboudian, R. *J. Am. Chem. Soc.* **2010**, *132*, 1476.
- (24) Wang, C. H.; Sun, D. C.; Xia, X. H. *Nanotechnology* **2006**, *17*, 651.
- (25) Fu, Y.; Lakowicz, J. R. *Laser Photonics Rev.* **2009**, *3*, 221.
- (26) Fu, Y.; Zhang, J.; Lakowicz, J. R. *Langmuir* **2007**, *24*, 3429.
- (27) Ray, K.; Badugu, R.; Lakowicz, J. R. *J. Am. Chem. Soc.* **2006**, *128*, 8998.
- (28) Ray, K.; Chowdhury, M. H.; Lakowicz, J. R. *Anal. Chem.* **2008**, *80*, 6942.
- (29) Malicka, J.; Gryczynski, I.; Gryczynski, Z.; Lakowicz, J. R. *Anal. Biochem.* **2003**, *315*, 57.
- (30) Gogoi, S. K.; Borah, S. M.; Dey, K. K.; Paul, A.; Chattopadhyay, A. *Langmuir* **2011**, *27*, 12263.
- (31) Zhang, L.; Chen, L.; Liu, H.; Hou, Y.; Hirata, A.; Fujita, T.; Chen, M. J. *Phys. Chem. C* **2011**, *115*, 19583.
- (32) Marmé, N.; Knemeyer, J.-P.; Sauer, M.; Wolfrum, J. *Bioconjugate Chem.* **2003**, *14*, 1133.
- (33) Wennmalm, S.; Edman, L.; Rigler, R. *Proc. Natl. Acad. Sci. U.S.A.* **1997**, *94*, 10641.
- (34) He, H.; Xie, C.; Ren, J. *Anal. Chem.* **2008**, *80*, 5951.
- (35) Geddes, C. D.; Parfenov, A.; Gryczynski, I.; Lakowicz, J. R. *J. Phys. Chem. B* **2003**, *107*, 9989.
- (36) Moskovits, M. *Nature* **2011**, *469*, 307.
- (37) Bek, A.; Jansen, R.; Ringler, M.; Mayilo, S.; Klar, T. A.; Feldmann, J. *Nano Lett.* **2008**, *8*, 485.